ACS Catalysis

Letter

Cite This: ACS Catal. 2018, 8, 75−80

pubs.acs.org/acscatalysis

Stable Pd-Doped Ceria Structures for CH_4 Activation and CO Oxidation

Ya-Qiong Su,[‡] Ivo A. W. Filot,[‡] Jin-Xun Liu, and Emiel J. M. Hensen*

Laboratory of Inorganic Materials Chemistry, Schuit Institute of Catalysis, Eindhoven University of Technology, P.O. Box 513, 5600 MB Eindhoven, The Netherlands

Supporting Information

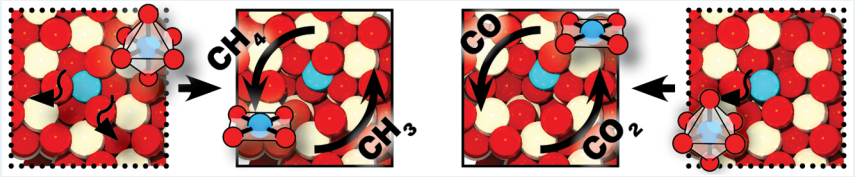

ABSTRACT: Doping CeO_2 with Pd atoms has been associated with catalytic CO oxidation, but current surface models do not allow CO adsorption. Here, we report a new structure of Pd-doped $CeO_2(111)$, in which Pd adopts a square planar configuration instead of the previously assumed octahedral configuration. Oxygen removal from this doped structure is favorable. The resulting defective Pd-doped CeO_2 surface is active for CO oxidation and is also able to cleave the first C−H bond in methane. We show how the moderate CO adsorption energy and dynamic features of the Pd atom upon CO adsorption and CO oxidation contribute to a low-barrier catalytic cycle for CO oxidation. These structures, which are also observed for Ni and Pt, can lead to a more open coordination environment around the doped-transition-metal center. These thermally stable structures are relevant to the development of single-atom catalysts.

KEYWORDS: *Pd-doped ceria, square planar PdO_4, CH_4 activation, CO oxidation, DFT*

Ceria (CeO_2) is a key component in environmental catalysis with main applications in the treatment of exhaust gases of combustion processes. The ability to reversibly store oxygen and the propensity to stabilize transition metals in high dispersion render CeO_2 a useful support for CO oxidation.[1−3] Pd is already used in three-way catalytic converter technology, because it is cheaper than Pt and Rh and its combination with CeO_2 results in excellent low-temperature CO oxidation activity.[4−8] Pd/CeO_2 is also an effective catalyst for the combustion of methane, which is of growing interest to avoid detrimental CH_4 slip from natural-gas powered combustion processes.[9,10]

For these oxidation reactions, the importance of a close interaction between Pd and CeO_2 has been stressed.[4,5,7,11] The identification of the nature of the active Pd sites in Pd/CeO_2 remains a considerable challenge. Ionic Pd in the surface or the bulk of ceria and metallic and oxidized Pd atoms, clusters, and nanoparticles on the surface have all been considered in this context.[4,5,7,11−15] Although metallic Pd nanoparticles on CeO_2 are active in CO oxidation,[13] high catalytic performance at low temperature has been linked to doping of Pd ions into the CeO_2 surface.[4,11] On the contrary, we recently showed that isolated PdO_x species are the active sites for low-temperature CO oxidation.[16] Gulyaev et al. contended that the active sites for CO oxidation are highly dispersed PdO_x clusters supported on a $Pd−CeO_2$ solid solution.[12]

For CH_4 oxidation, the role of ionic Pd has also been discussed.[8,17] Trovarelli and co-workers suggested that the active sites are isolated square planar PdO_4 moieties in the CeO_2 surface.[8,17] Lu and co-workers mentioned that ionic Pd in CeO_2 is more active than PdO on CeO_2.[18] Tao and co-workers reported the promise of transition-metal dopants in CeO_2 for CH_4 oxidation.[19] Thus, it is important to determine the way CH_4 is activated on Pd-doped CeO_2.

Determining the location of highly dispersed Pd in or on the CeO_2 surface remains an experimental challenge.[5,17,20] Priolkar et al. used EXAFS to show that Pd in Pd/CeO_2, prepared by a one-step solution combustion method, coordinates to only three O atoms.[5] Watson and co-workers reported that Pd and Pt prefer a square planar coordination in the bulk of CeO_2, in which each Pd atom is coordinated by four O atoms.[21,22] Boronin and co-workers suggested that Pd^{2+} ions retain a nearly square planar coordination in $Pd_xCe_{1-x}O_{2-x-\sigma}$ solid solutions.[20] Quantum-chemical modeling can aid in determining the catalytic role of candidate structures of Pd-doped CeO_2. The most stable structure identified for single-atom Pd-doped CeO_2 involves replacement of a surface Ce atom by Pd,[23−26] which results in octahedral Pd species. A problem of this proposed structure is that it cannot adsorb CO.[11]

We identified by state-of-the-art density functional theory (DFT) a novel stable structure for a single Pd atom doped in the $CeO_2(111)$ surface. This structure is different from the octahedral configuration that has been previously considered to

Received: September 25, 2017
Revised: October 24, 2017
Published: November 20, 2017

DOI: 10.1021/acscatal.7b03295
ACS Catal. 2018, 8, 75−80

be the most stable structure of Pd-doped $CeO_2(111)$.[11,23−29] We will show that removal of surface oxygen is easier from the square planar Pd-doped $CeO_2(111)$ structure than from the octahedral Pd-doped $CeO_2(111)$ one. This results in increased CH_4 activation. While octahedrally coordinated Pd in ceria cannot adsorb CO, a low-barrier catalytic cycle for CO oxidation was found for the new structure, in which the flexibility of Pd upon CO adsorption and surface O atoms feature prominently.

The initial surface model was constructed by replacing a Ce atom by a Pd atom in the (111) surface of CeO_2. This substitution is favorable (ΔE = −3.62 eV), in line with the literature.[25] The resulting structure corresponds to the previously identified configuration in which Pd is octahedrally coordinated (Pd-dop-I in Figure 1). The energy to create an O

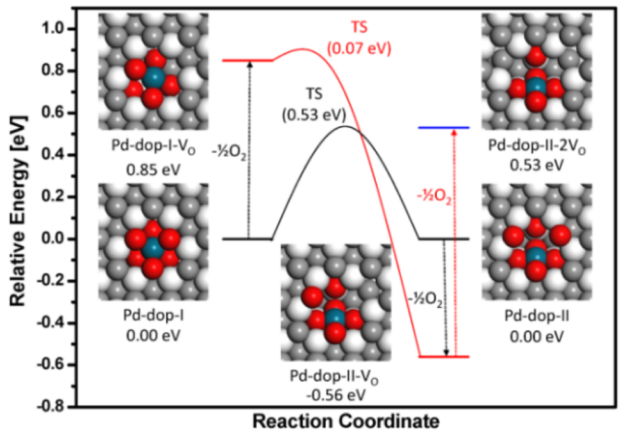

Figure 1. Potential energy diagram for the transformation between the previously most stable stoichiometric Pd-dop-I and defective Pd-dop-I-V_O structures and the herein found Pd-dop-II, Pd-dop-II-V_O, and Pd-dop-II-2V_O structures of Pd-doped $CeO_2(111)$ (color code: white, Ce; gray, irrelevant O; red, relevant O; green, Pd).

vacancy (V_O) for Pd-dop-I (ΔE = 0.85 eV) is much lower than for the stoichiometric $CeO_2(111)$ surface (ΔE = 2.24 eV),[30,31] reflecting the weaker bonding of a surface O atom to Pd in comparison to Ce.[24] Pd adopts a square planar coordination in the resulting defective Pd-dop-I-V_O structure in which two O atoms lie in top surface, and the other two in the second O layer (Figure S2).

As the EXAFS study of Priolkar et al. suggested the existence of a stable structure with a lower Pd−O coordination,[5] we carefully explored alternative structures of the Pd-doped CeO_2 surface. This resulted in the identification of a stoichiometric Pd-dop-II structure shown in Figure 1, in which the Pd atom is coordinated in a square planar manner by four O atoms, i.e., one surface O atom, two subsurface O atom, and one O atom in the third atomic layer of CeO_2 with respective Pd−O bond lengths of 1.92, 2.01, and 1.97 Å. This square planar Pd configuration can be obtained from the octahedral Pd-dop-I structure by a surface reconstruction, which involves a small barrier of only 0.53 eV. Pd-dop-I and Pd-dop-II are equally stable.

A square planar structure has already been reported for Pd doped in the less stable $CeO_2(100)$ surface and the bulk of CeO_2.[21,22,32,33] It is important to stress that this already known structure resembles Pd-dop-I-V_O. The structure of Pd-doped-II is different from these structures as highlighted in Figure S2.

Different from Pd-dop-I, the formation of an O vacancy in Pd-dop-II is exothermic (ΔE = −0.56 eV). This is important, because the resulting defective structure Pd-dop-II-Vo is strongly thermodynamically favored over Pd-dop-I and its defective counterpart Pd-dop-I-V_O. Figure 1 also shows that Pd-dop-I-V_O is metastable, as it can very easily transform into the much more stable Pd-dop-II-V_O structure (E_{act} = 0.07 eV). The removal of a second O atom from Pd−V_O-II to obtain Pd-dop-II-2V_O is unfavorable (ΔE = +1.09 eV). This energy is, however, still much lower than the energy required to create an O vacancy in the stoichiometric $CeO_2(111)$ surface. By removing the second O atom, two Ce^{3+} ions are formed.

In order to determine the stability of the various structures as a function of temperature and O_2 partial pressure, we carried out an ab initio thermodynamics analysis. The resulting phase diagram in Figure 2 shows that Pd-dop-II-V_O is the most stable

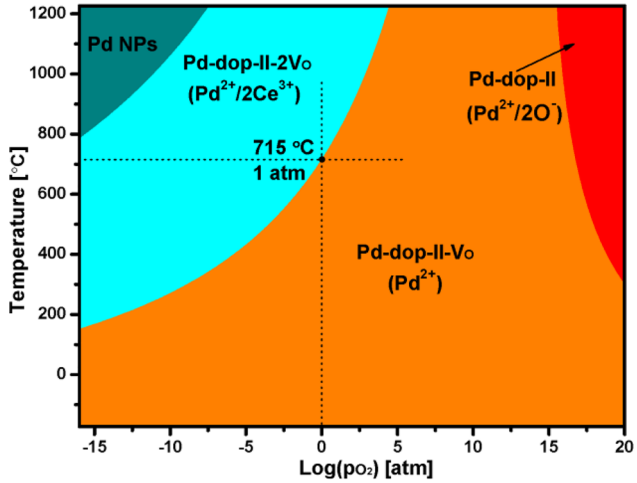

Figure 2. Diagram showing the stability of different Pd-doped $CeO_2(111)$ surface structures as a function of the temperature and the O_2 pressure based on an ab initio thermodynamic analysis using first-principles DFT data.

structure at typical temperatures and in an oxygen atmosphere. The fully oxidized Pd-doped surface (Pd-dop-II) is only stable at very high O_2 pressure. The removal of another O atom from Pd-dop-II-V_O will occur at very high temperature (T > 715 °C at 1 atm O_2 pressure). Removal of more O atoms from Pd-dop-II-2V_O is even less favorable, costing more than the removal of O from the stoichiometric $CeO_2(111)$ surface. This suggests that a single Pd atom embedded in the $CeO_2(111)$ surface is very stable. Based on the oxygen vacancy formation energies, we can estimate under which conditions the O atoms close to Pd can be removed (see the Supporting Information). This would lead to the reduction of Pd, after which Pd can easily diffuse over the ceria surface and form metallic Pd clusters or large nanoparticles (NPs).[34] It is seen in Figure 2 that this process is thermodynamically only possible above 800 °C at practical oxygen pressures, in agreement with experimental observation.[35] We also found that Pd embedded in a Ce vacancy of $CeO_2(111)$ is 1.94 eV more stable than in a Pd vacancy of PdO(101) (Figure S3). This shows that Pd will not segregate from its location in the $CeO_2(111)$ surface under practical conditions.

In order to gain an understanding of the electronic structure of Pd-doped $CeO_2(111)$, we studied the partial density of states (pDOS) for Pd-dop-I, Pd-dop-II, and Pd−V_O-II. Figure 3

DOI: 10.1021/acscatal.7b03295
ACS Catal. 2018, 8, 75−80

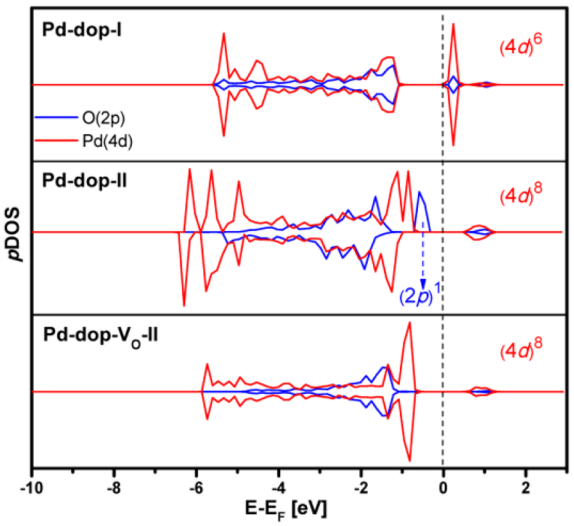

Figure 3. Partial density of states (*p*DOS) of Pd-4d and O-2p orbitals (O atom adjacent to Pd) in Pd-dop-I, Pd-dop-II, and Pd-dop-II-V_O.

presents the partial DOS for the Pd atom and the adjacent O atom. There are no Ce^{3+} ions in Pd-dop-I, implying that Pd is in the +4 oxidation state. This is also reflected by the unoccupied Pd-4d state located slightly above the Fermi level. These states become occupied in the Pd-dop-II structure, corresponding to the formal reduction of Pd^{4+} to Pd^{2+}. This reduction is related to the cleavage of two of the Pd−O bonds, which results in electron transfer from the lattice O atoms to Pd. The changes in the geometric and electronic structures are corroborated by the increasing Pd−O bond lengths for these two O atoms and the appearance of an unpaired electron in one of the 2p orbitals of the lattice O atoms. The radical character of these two O atoms is also evident from their magnetic moment of 0.534 μ_B. As no Ce 4f states are filled, the Pd atom is in the +2 oxidation state. Finally, the removal of one of these two O atoms to obtain Pd-dop-II-V_0 results in the conversion of the other O^- ion to an O^{2-} ion, as follows from the disappearance of the occupied 2p state in the DOS. When the second O atom is removed, two Ce^{4+} ions are reduced to the +3 state, meaning that the Pd atom maintains the +2 oxidation state. The oxidation states of the two Pd configurations are in line with crystal ligand field theory, which predicts that Pd^{4+} (d^6) is preferentially octahedrally coordinated by O and that Pd^{2+} (d^8) prefers to reside in a square planar oxygen coordination environment.[36]

We then explored the reactivity of the various Pd-doped CeO_2 surface models toward the first C−H bond in CH_4. In this step, CH_4 directly reacts with a surface O atom to form a methyl radical and a surface hydroxyl species.[37] Table 1 shows that CH_4 only weakly interacts with the surface. Therefore, C−H bond activation will follow an Eley−Rideal mechanism. The activation energies with respect to the gas phase for Pd-dop-I, Pd-dop-II, Pd-dop-II-V_O, and the stoichiometric $CeO_2(111)$ surface are 0.75, 0.12, 0.83, and 1.36 eV, respectively. The activation energy is 1.14 eV for C−H activation by the O atom bound to Pd in Pd-dop-II-$2V_O$, similar to the value of 1.22 eV for the PdO(100) surface.[38] For all of the transition states, the C−H and O−H bond lengths are between 1.13 and 1.45 Å, and the C−H−O valence angle is around 170°. After CH_4 dissociation, the H atom binds to a surface lattice O atom and the CH_3 radical will diffuse to another surface O atom. The

Table 1. Adsorption energies (E_{ads}) and Activation Energies (E_{act}) with Respect to the Gas Phase, Reaction Rate Constants k for C−H Bond Activation in CH_4, and Abundance F of the Various Surface Models[a]

surface sites	E_{ads} (eV)	E_{act} (eV)	k (s^{-1})	F
$CeO_2(111)$	−0.18	1.36	5.25×10^{-14}	-
Pd-dop-I	−0.17	0.75	1.29×10^{-9}	0.0183
Pd-dop-II	−0.15	0.12	5.25×10^{-5}	<0.001
Pd-dop-II-V_O	−0.16	0.83	2.91×10^{-10}	0.979
Pd-dop-II-$2V_O$	−0.19	1.14	2.01×10^{-12}	0.0025

[a] P_{CH_4} = 0.1 atm, P_{O_2} = 1 atm, and T = 700 K.

activation energy of 1.36 eV for the stoichiometric $CeO_2(111)$ model agrees with the value reported in the literature.[39,40] Clearly, C−H bond activation in CH_4 is most favorable on Pd-dop-II. The more stable Pd-dop-II-V_O structure presents an activation barrier of 0.83 eV, still much lower than that for the stoichiometric $CeO_2(111)$ surface and close to the value computed for the Pd-dop-I surface model. The reaction rates predicted for dissociative CH_4 adsorption are listed in Table 1. Although Pd-dop-II shows the highest intrinsic activity, its low abundance under typical reaction conditions implies that its contribution to CH_4 activation will be negligible. Despite the fact that Pd-dop-I and Pd-dop-II-V_O exhibit comparable rates, the much higher abundance of Pd-dop-II-V_O means that this state is the dominant catalytically active species for CH_4 activation, in line with the suggestion of Trovarelli and co-workers.[17] A more detailed analysis shows that the activation energy of dissociative CH_4 adsorption strongly correlates with the oxygen vacancy formation energy (Figure S6). The more weakly an O atom is bound to the surface the lower the activation energy for CH_4 activation. The most reactive atom is the unstable O atom adjacent to Pd dopant in Pd-dop-II, the least a ceria surface O atom.

As it has been speculated that Pd atoms doped in CeO_2 play an important role in CO oxidation,[4,5,11,15] we also explored possible reaction cycles for CO oxidation to CO_2. Figure 4 shows the free energy pathways computed at 300 K. The conventional structure cannot catalyze CO oxidation as the Pd atom does not adsorb CO.[11] In contrast, CO can adsorb on the Pd ion in Pd-dop-II (IM1 → IM2) with an energy of −0.58 eV. The oxidation of CO by a CeO_2 lattice O atom is facile, and the activation energy is only 0.03 eV. CO_2 desorption (IM3 → IM4) is exergonic by 1.33 eV. Adsorption of a subsequent CO molecule (IM4 → IM5, ΔG = −0.36 eV) results in surface reorganization, in which Pd migrates to the first atomic (O) layer of the surface, after which Pd is surrounded by two surface O, one subsurface O, and CO. This CO molecule will react with one of the O atoms in the second O atomic layer (IM5 → IM6) involving an activation barrier of 0.61 eV. This reaction is slightly preferred over the reaction with a surface O atom (IM5 → IM6′, E_{act} = 0.73 eV). After CO_2 desorption (IM6 → IM7, ΔG = −0.78 eV), the preferred square planar coordination is restored with one V_O in the first O atomic layer and one V_O in the second O atomic layer, denoted by Pd-dop-II-$2V_O$-sub. Then, O_2 adsorption (IM7 → IM8) occurs with ΔG = −1.14 eV followed by dissociation (IM8 → IM1) with E_{act} = 1.52 eV. Alternatively, CO adsorption (IM7 → IM9, ΔG = −0.13 eV) results in surface reorganization and reaction with a surface O atom (IM9 → IM10) to form another CO_2 with a barrier of 0.73 eV. This process is exergonic (ΔG = −1.99 eV), and CO_2 desorption (IM10 → IM11, ΔG = 0.35 eV) leads to Pd-dop-II-

DOI: 10.1021/acscatal.7b03295
ACS Catal. 2018, 8, 75−80

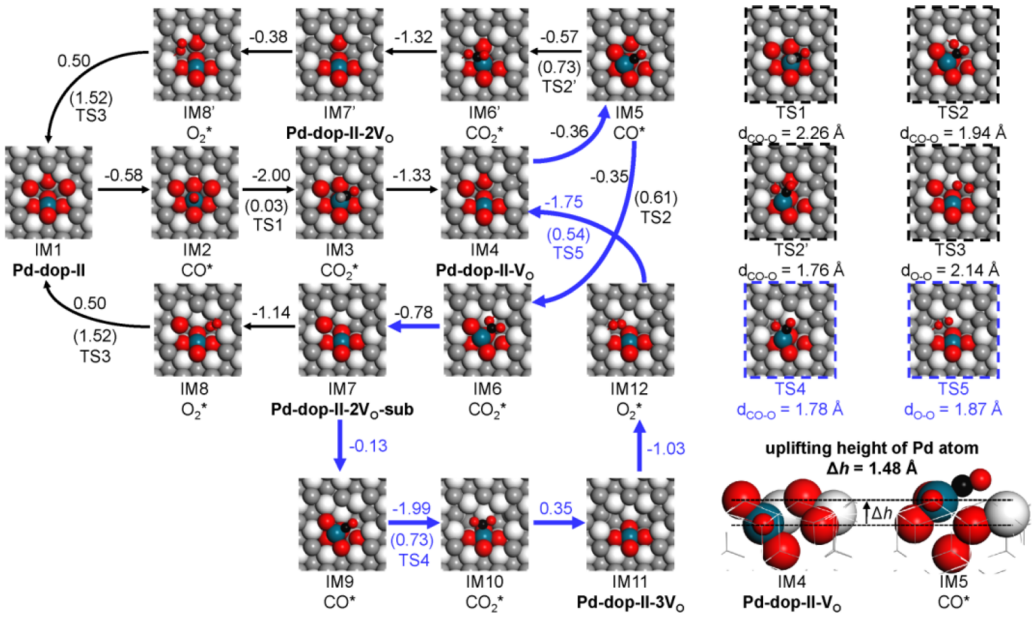

Figure 4. Free energy (in eV) pathways for CO oxidation by Pd-doped $CeO_2(111)$ at T = 300 K (free energy computed by considering the entropies of gas phase species; the numbers in parentheses are activation energies). Transition states are indicated by the dashed blue/black lines (color code: white, Ce; gray, irrelevant O; red, relevant O; black, C; green, Pd).

$3V_O$, a structure with three O vacancies, two in the first O atomic layer and one in the second O atomic layer. Adsorption of molecular O_2 (IM11 → IM12, $\Delta G = -1.03$ eV) followed by dissociation (IM12 → IM4; $E_{act} = 0.54$ eV) results in healing of the two O vacancies, thereby restoring Pd-dop-II-V_O. We also considered the alternative pathway: after CO_2 desorption occurs from the IM6′ state to form Pd-dop-II-$2V_O$, O_2 adsorption (IM7′ → IM8′) is slightly exergonic by −0.38 eV and involves a barrier of 1.52 eV for O_2 dissociation.

Microkinetics simulations were used to identify the preferred reaction pathway under practical conditions. In this way, we found that CO is predominantly oxidized via the sequence (IM4 → IM5 → ... → IM11 → IM12), which starts from Pd−II−V_O and involves the removal of two O atoms before O_2 heals these two vacancies. The CO oxidation rate of this cycle at 300 K is $\sim 10^9$ and $\sim 10^6$ times higher than the two cycles starting from Pd-dop-II, i.e., IM1 → IM8 and IM1 → IM8′, respectively. The rate-controlling step for the overall process is the second CO oxidation event (IM9 → IM10). The rate of the other two cycles is mainly suppressed by the high barrier to O_2 dissociation. The key aspects of the dominant catalytic cycle are the relatively weak adsorption of CO, which leads to moderate activation barriers for recombination with the lattice O atoms in the first and second O atomic layers of CeO_2, and the uplifting out of the surface of the Pd atom from its initial location upon CO adsorption. This reorganization around the active Pd center facilitates the recombination of CO with an O atom. Figure S10 highlights the role of adsorbed CO in this reorganization process. This is the first reported catalytic cycle for CO oxidation of a single Pd atom doped in the $CeO_2(111)$surface. The predicted rate is several orders of magnitude lower than the computed rate of CO oxidation by an isolated PdO species supported on the $CeO_2(111)$ surface.[16] Thus, we conclude that a single metal atom PdO species supported on the surface is a more active CO oxidation catalyst than a single Pd atom embedded in the $CeO_2(111)$ surface.

To verify the generality of the predicted square-planar structure, we considered similar structures with Ni and Pt, which are the other important group 10 elements used in combination with ceria for CH_4 activation.[39,41,42] Figure 5 shows the corresponding potential energy diagrams (cf. Figure 1). Ni, Pd, and Pt can form similar square planar structures. Their stability increases going from Pt < Pd < Ni. Only the stoichiometric square planar Pt structure is slightly less stable than the octahedral one. Yet, in all cases, it is favorable to remove an O atom from the square planar structure. These structures are always more stable than those obtained by removing an O atom from the octahedral structure. Notably, doing so for Ni-dop-I leads to an unstable structure that transforms without barrier to Ni-dop-II-V_O, consistent with the high stability of this structure.

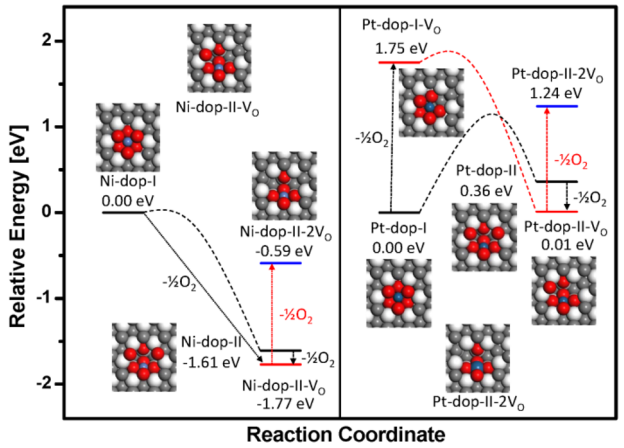

Figure 5. Potential energy diagrams for the transformation between stoichiometric and defective Ni- and Pt-dop-I and Ni- and Pt-dop-II structures (color code: white, Ce; gray, irrelevant O; red, relevant O; green, Pt; blue, Ni).

DOI: 10.1021/acscatal.7b03295
ACS Catal. 2018, 8, 75−80

In conclusion, we have used quantum-chemical calculations to identify an alternative structure for a single Pd atom doped in the most stable surface termination of CeO_2. Compared with the conventional octahedrally coordinated PdO_6 moiety, the novel square planar PdO_4 structure is more reactive due to the radical character of the two surface O atoms. Creating a vacancy in this square planar structure is energetically favorable, and the resulting defective surface is the most stable structure under oxidative conditions. Similar structures exist for the Ni- and Pt-doped surfaces. A surface O atom nearby the Pd dopant can easily activate the first C−H bond in CH_4. In contrast to octahedrally coordinated Pd, the square planar configuration can adsorb CO. The relatively weak CO adsorption results in moderate activation barriers for recombination with the O atoms of CeO_2. The novel structure identified in this study paves the way for deeper exploration and optimization of CeO_2 surfaces toward single-atom catalysts with high activity and stability.

■ ASSOCIATED CONTENT

Supporting Information

The Supporting Information is available free of charge on the ACS Publications website at DOI: 10.1021/acscatal.7b03295.

Partition function of gaseous CH_4, computational details, ab initio thermodynamic analysis, additional structural information, and results of microkinetics modeling (PDF)

■ AUTHOR INFORMATION

Corresponding Author

*E-mail:e.j.m.hensen@tue.nl.

ORCID

Ivo A. W. Filot: 0000-0003-1403-8379

Jin-Xun Liu: 0000-0002-7499-4197

Emiel J. M. Hensen: 0000-0002-9754-2417

Author Contributions

‡(Y.-Q.S. and I.A.W.F.) These authors contributed equally.

Notes

The authors declare no competing financial interest.

■ ACKNOWLEDGMENTS

The authors acknowledge financial support for the research from The Netherlands Organization for Scientific Research (NWO) through a Vici grant and Nuffic funding. Supercomputing facilities were provided by NWO.

■ REFERENCES

(1) Zheng, T.; He, J.; Zhao, Y.; Xia, X.; He, J. *J. Rare Earths* **2014**, *32*, 97−107.

(2) Jen, H. W.; Graham, G. W.; Chun, W.; McCabe, R. W.; Cuif, J. P.; Deutsch, S.; Touret, O. *Catal. Today* **1999**, *50*, 309−328.

(3) Yao, H.; Yao, Y. *J. Catal.* **1984**, *86*, 254−265.

(4) Li, G.; Li, L.; Jiang, D. *J. Phys. Chem. C* **2015**, *119*, 12502−12507.

(5) Priolkar, K. R.; Bera, P.; Sarode, P. R.; Hegde, M. S.; Emura, S.; Kumashiro, R.; Lalla, N. P. *Chem. Mater.* **2002**, *14*, 2120−2128.

(6) Bera, P.; Patil, K. C.; Jayaram, V.; Subbanna, G. N.; Hegde, M. S. *J. Catal.* **2000**, *196*, 293−301.

(7) Boronin, A. I.; Slavinskaya, E. M.; Danilova, I. G.; Gulyaev, R. V.; Amosov, Yu. I.; Kuznetsov, P. A.; Polukhina, I. A.; Koscheev, S. V.; Zaikovskii, V. I.; Noskov, A. S. *Catal. Today* **2009**, *144*, 201−211.

(8) Trovarelli, A. *Catal. Rev.: Sci. Eng.* **1996**, *38*, 439−520.

(9) Mansor, M. R. A.; Abbood, M. M.; Mohamad, T. I. *Fuel* **2017**, *190*, 281−291.

(10) Sharma, S.; Ghoshal, S. K. *Renewable Sustainable Energy Rev.* **2015**, *43*, 1151−1158.

(11) Liu, J.; Liu, B.; Fang, Y.; Zhao, Z.; Wei, Y.; Gong, X. Q.; Xu, C.; Duan, A.; Jiang, G. *Environ. Sci. Technol.* **2014**, *48*, 12403−12410.

(12) Gulyaev, R. V.; Slavinskaya, E. M.; Novopashin, S. A.; Smovzh, D. V.; Zaikovskii, A. V.; Osadchii, D. Yu.; Bulavchenko, O. A.; Korenev, S. V.; Boronin, A. I. *Appl. Catal., B* **2014**, *147*, 132−143.

(13) Fernández-Garcıa, M.; Martınez-Arias, A.; Salamanca, L. N.; Coronado, J. M.; Anderson, J. A.; Conesa, J. C.; Soria, J. *J. Catal.* **1999**, *187*, 474−485.

(14) Hinokuma, S.; Fujii, H.; Katsuhara, Y.; Ikeue, K.; Machida, M. *Catal. Sci. Technol.* **2014**, *4*, 2990−2996.

(15) Kurnatowska, M.; Kepinski, L.; Mista, W. *Appl. Catal., B* **2012**, *117*, 135−147.

(16) Spezzati, G.; Su, Y. Q.; Hofmann, J. P.; Benavidez, A. D.; Delariva, A. T.; McCabe, J.; Datye, A. K.; Hensen, E. J. M. *ACS Catal.* **2017**, *7*, 6887−6891.

(17) Colussi, S.; Gayen, A.; Camellone, M. F.; Boaro, M.; Llorca, J.; Fabris, S.; Trovarelli, A. *Angew. Chem., Int. Ed.* **2009**, *48*, 8481−8484.

(18) Meng, L.; Lin, J.-J.; Pu, Z. Y.; Luo, L. F.; Jia, A.-P.; Huang, W. X.; Luo, M. F.; Lu, J. Q. *Appl. Catal., B* **2012**, *119*, 117−122.

(19) Zhu, Y.; Zhang, S.; Shan, J. J.; Nguyen, L.; Zhan, S.; Gu, X.; Tao, F. *ACS Catal.* **2013**, *3*, 2627−2639.

(20) Gulyaev, R.; Kardash, T. Y.; Malykhin, S.; Stonkus, O.; Ivanova, A.; Boronin, A. *Phys. Chem. Chem. Phys.* **2014**, *16*, 13523−13539.

(21) Scanlon, D. O.; Morgan, B. J.; Watson, G. W. *Phys. Chem. Chem. Phys.* **2011**, *13*, 4279−4284.

(22) Kehoe, A. B.; Scanlon, D. O.; Watson, G. W. *Chem. Mater.* **2011**, *23*, 4464−4468.

(23) Mayernick, A. D.; Janik, M. J. *J. Catal.* **2011**, *278*, 16−25.

(24) Mayernick, A. D.; Janik, M. J. *J. Phys. Chem. C* **2008**, *112*, 14955−14964.

(25) Ding, W. C.; Gu, X. K.; Su, H. Y.; Li, W. X. *J. Phys. Chem. C* **2014**, *118*, 12216−12223.

(26) Guo, C.; Wei, S.; Zhou, S.; Zhang, T.; Wang, Z.; Ng, S. P.; Lu, X.; Wu, C. L.; Guo, W. *ACS Appl. Mater. Interfaces* **2017**, *9*, 26107−26117.

(27) Zhao, Y.; Teng, B.-T.; Wen, X.-D.; Zhao, Y.; Zhao, L.-H.; Luo, M. F. *Catal. Commun.* **2012**, *27*, 63−68.

(28) Mayernick, A. D.; Janik, M. J. *J. Chem. Phys.* **2009**, *131*, 084701.

(29) Krcha, M. D.; Mayernick, A. D.; Janik, M. J. *J. Catal.* **2012**, *293*, 103−115.

(30) Su, Y. Q.; Filot, I. A. W.; Liu, J. X.; Tranca, I.; Hensen, E. J. M. *Chem. Mater.* **2016**, *28*, 5652−5658.

(31) Li, H. Y.; Wang, H. F.; Gong, X. Q.; Guo, Y. L.; Guo, Y.; Lu, G.; Hu, P. *Phys. Rev. B: Condens. Matter Mater. Phys.* **2009**, *79*, 193401.

(32) Figueroba, A.; Bruix, A.; Kovács, G.; Neyman, K. M. *Phys. Chem. Chem. Phys.* **2017**, *19*, 21729−21738.

(33) Figueroba, A.; Kovács, G.; Bruix, A.; Neyman, K. M. *Catal. Sci. Technol.* **2016**, *6*, 6806−6813.

(34) Su, Y. Q.; Liu, J. X.; Filot, I. A. W.; Hensen, E. J. M. *Chem. Mater.* **2017**, *29*, 9456−9462.

(35) Cargnello, M.; Jaén, J. D.; Garrido, J. H.; Bakhmutsky, K.; Montini, T.; Gámez, J. C.; Gorte, R.; Fornasiero, P. *Science* **2012**, *337*, 713−717.

(36) Senftle, T. P.; van Duin, A. C.; Janik, M. J. *ACS Catal.* **2015**, *5*, 6187−6199.

(37) Chin, Y. H.; Buda, C.; Neurock, M.; Iglesia, E. *J. Am. Chem. Soc.* **2013**, *135*, 15425−15442.

(38) Hellman, A.; Resta, A.; Martin, N.; Gustafson, J.; Trinchero, A.; Carlsson, P. A.; Balmes, O.; Felici, R.; van Rijn, R.; Frenken, J.; et al. *J. Phys. Chem. Lett.* **2012**, *3*, 678−682.

(39) Tang, W.; Hu, Z.; Wang, M.; Stucky, G. D.; Metiu, H.; McFarland, E. W. *J. Catal.* **2010**, *273*, 125−137.

(40) Senftle, T. P.; van Duin, A. C.; Janik, M. J. *ACS Catal.* **2017**, *7*, 327−332.

DOI: 10.1021/acscatal.7b03295
ACS Catal. 2018, 8, 75−80

(41) Zhang, S.; Muratsugu, S.; Ishiguro, N.; Tada, M. *ACS Catal.* **2013**, *3*, 1855−1864.
(42) Lustemberg, P. G.; Ramírez, P. J.; Liu, Z.; Gutiérrez, R. A.; Grinter, D. G.; Carrasco, J.; Senanayake, S. D.; Rodriguez, J. A.; Ganduglia-Pirovano, M. V. *ACS Catal.* **2016**, *6*, 8184−8191.

DOI: 10.1021/acscatal.7b03295
ACS Catal. 2018, 8, 75−80